Real-time terahertz imaging over a standoff distance (>25 meters)

Alan W. M. Lee,[a] Qi Qin, Sushil Kumar, Benjamin S. Williams, and Qing Hu
Research Laboratory of Electronics, Department of Electrical Engineering and Computer Science, Massachusetts Institute of Technology, Cambridge, Massachusetts 02139

John L. Reno
Department 1123, Sandia National Laboratories, MS 1303, Albuquerque, New Mexico 87185-1303

(Received 2 August 2006; accepted 28 August 2006; published online 6 October 2006)

The authors demonstrate the use of a terahertz quantum cascade laser (QCL) for real-time imaging in transmission mode at a standoff distance of 25 meters. Lasing frequency was selected for optimum transmission within an atmospheric window at ~4.9 THz. Coarse frequency selection was made by design of the QCL gain medium. Finer selection (to within 0.1 THz) was made by judicious choice of laser cavity length to adjust facet losses and therefore lasing threshold bias, in order to overlap the peak frequency of the Stark-shifted gain spectrum with the atmospheric window. Images are shown using an uncooled 320×240 microbolometer camera. © *2006 American Institute of Physics*. [DOI: 10.1063/1.2360210]

Terahertz (0.3–10 THz) imaging has been demonstrated for applications such as illicit drug detection[1] and through package inspection.[2] To be of practical use, real-time operation will be necessary, requiring multimilliwatt sources and focal-plane array detectors. Because of distinctive terahertz spectral "fingerprints" found in many chemical compounds, terahertz sensing and imaging could have important military and security applications.[3] For these applications, imaging at a standoff distance (~10–25 m) is essential. However, water vapor strongly absorbs radiation at terahertz frequencies, which results in heavy atmospheric attenuation, >10 dB/m, outside of isolated low-loss transmission windows, which are only a few hundred gigahertz wide. These narrow transmission bands favor the use of narrow band sources. Far-infrared gas lasers are bulky and power hungry, and they have only limited selection of lasing frequencies. Schottky-diode frequency multipliers can only produce submilliwatt power levels at $f>1$ THz and are not suitable for illuminating focal-plane arrays for real-time imaging. By comparison, terahertz quantum cascade lasers (QCLs) have demonstrated peak power levels of ~250 mW in pulsed and ~130 mW in cw operations.[4] Their intersubband-transition nature implies that any desired frequency can be achieved by band gap and waveguide engineering over a continuous frequency range from 1.59 to 5 THz, over which these lasers have been demonstrated.[5] Previously we demonstrated the feasibility of real-time terahertz imaging using an ~50 mW peak power, 4.31 THz QCL operating at ~30 K, which is the temperature of a cryogen-free thermomechanical cryocooler. This power level was sufficient for producing a signal to noise ratio (SNR) of 340 when used with a commercial 320×240 pixel microbolometer array[6] over a short distance of ~30 cm. In this letter, we demonstrate the use of a frequency optimized terahertz QCL for real-time imaging in transmission mode over a standoff distance of 25.8 m.

In order to develop the long-range capability of terahertz imaging, it is important and instructive to analyze the effect of several laser characteristics, most importantly the output power level and frequency, on the power received at the end of the standoff range. Because of the exponential decay of transmitted power through space, for a given minimum detectable power, the incremental distance Δl between the transmitter and the detector changes only *logarithmically* with the power available at the transmitter, $\Delta l = (10 \log N)/\alpha$, where N is the N-fold increase in power and α is the atmospheric attenuation coefficient in dB/m. The frequency dependence of α is shown in Fig. 1, and it changes rapidly and nonmonotonically in the terahertz range, often varying by several dB/m over a span of ~0.1 THz. For typical values of α at terahertz frequencies ranging from 0.5 to 10 dB/m, a tenfold increase in power yields diminishing increases in the range from 20 to 1 m. Again, because of the exponential decay, a small change in α will result in a significant change of the transmitted power over a long distance. Numerically, the relative transmitted power over 25 m is 0.32% for $\alpha=1$ dB/m but is 5.6% for $\alpha=0.5$ dB/m. This straightforward but important analysis dictates that for long-range terahertz imaging, the frequency of the transmitter is much more important than its power, as long as adequate power levels (>10 mW) are available. This observation has

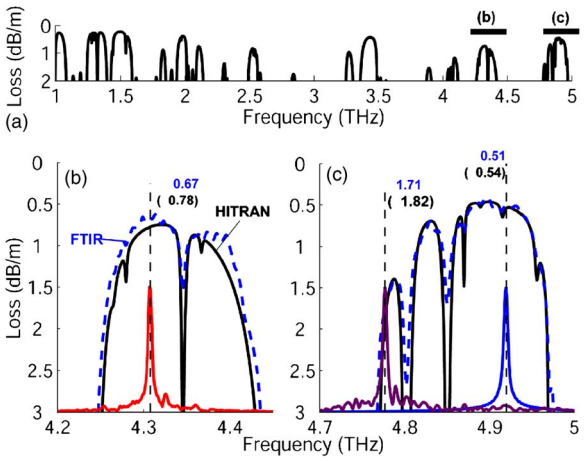

FIG. 1. (Color online) Atmospheric path loss in dB/m, measured by FTIR (dashed) and calculated from HITRAN 2004 (solid) at 296 K and 40% relative humidity for continuous frequency range of 1–5 THz [part (a) calculation only] and 4.3 and 4.9 THz windows [parts (b) and (c)]. Measured (calculated) path loss indicated at lasing frequencies of several selected QCL devices, shown with lasing spectra of devices in text (amplitude in a.u.).

[a]Electronic mail: awmlee@mit.edu

been the guiding principle of the reported work.

In this work, we are focused on the frequency range of 4–5 THz, in which we have developed QCLs with the highest output power levels. The aforementioned high-power laser at ~4.3 THz has produced adequate results in real-time imaging over a distance of ~10 m. However, the quality of the imaging degraded noticeably at the longer 25 m range. Upon a close inspection of Figs. 1(b) and 1(c), it is clear that the atmospheric window at ~4.9 THz has lower attenuation and therefore is more desirable for long-range imaging. Quantitatively, the measured atmospheric attenuations are 0.51 and 0.67 dB/m, at 4.92 and 4.31 THz, respectively. While these attenuations cause comparable losses over short ranges, they increase exponentially with distance. For example, at ranges of 25 and 100 m, the 4.92 THz window results in 2.5 and 40 times more transmitted power, respectively. Furthermore, α increases linearly with the absolute humidity, and thus at higher humidities these differences become even greater. Atmospheric transmission measurements were taken by Fourier transform infrared spectrometer with a resolution of 3.75 GHz, in the laboratory environment of 296 K and 40% relative humidity (RH), over a 1.3 m path length using a 1000 K SiC blackbody source with a deuterated triglycine sulfate detector. The amplitude was normalized to a spectrum taken under nitrogen purge. These values are compared in Fig. 1 with calculated values from the HITRAN 2004 database[7] under the same conditions, modeling atmospheric water ($H_2{}^{16}O$, 99.7% abundant), with additional terahertz transmission windows shown from 1 to 5 THz.

The QCL device (labeled FL179R-M1) is based on the resonant-phonon active region, which uses a combination of resonant tunneling and fast LO-phonon scattering to achieve population inversion.[8] The device used in this work is similar in design to the 4.31 THz, high-power device described in Ref. 4 (labeled FL183R-2, spectrum shown in Fig. 1). To increase the emission frequency, the radiative barrier was thinned from 17 to 15.5 Å, increasing the energy separation (anticrossing) between the upper and lower radiative states to 20.3 meV (~4.9 THz) at design bias. In order to reduce a parasitic current channel, we also thickened the injection barrier from 48 to 54 Å, which resulted in a reduction of the threshold current density. However, this thicker injection barrier also reduced the maximum current density and yielded a lower power level (by a factor of ~3) from the previous device. The active region was grown by molecular beam epitaxy and processed into semi-insulating surface plasmon Fabry-Pérot ridge waveguides of various geometries using dry etching, with the rear facets high-reflectivity coated.

A number of devices with a width of 100 μm and lengths from 3.05 to 1.97 mm long were tested. The ridge width was chosen to optimize peak optical power output while maintaining efficient heat removal laterally through the substrate. A continuous-wave (cw) spectrum of a 3.05 mm long device is shown in Fig. 1 and is typical of the longer devices, which emit near ~4.77 THz. As shown in Fig. 1(c), the atmospheric attenuation at this particular frequency is quite high (~1.8 dB/m). In order to shift the lasing frequency to the desired ~4.9 THz, we deliberately selected devices with waveguide geometries that have higher lasing thresholds and therefore marginally lower power levels. Shorter lengths were used in order to increase the facet loss α_m, which is inversely proportional to the cavity length. The increase in loss results in a higher electrical bias at lasing threshold and a concomitant blue Stark shift of the gain spectrum. In our vertical-transition laser device and above the lasing threshold, the additional bias voltage mostly drops outside the active region because of gain clamping.[9] As a result, the emission frequency is effectively set at the threshold. The cw spectrum of the 1.97 mm long device used in this work is shown in Fig. 1, emitting around 4.92 THz which is quite close to the optimum frequency in the ~4.9 THz window.

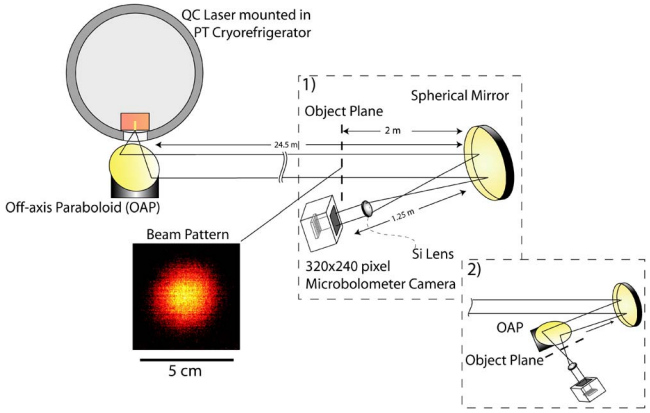

FIG. 2. (Color online) Experimental setup for imaging over a distance of 25.75 m. A QCL device is mounted in a pulse-tube cryocooler, with emitted beam collimated by an off-axis paraboloid mirror, for transmission over a 24.5 m path before collection by a 15 cm diameter spherical mirror. In configuration (1), an object is placed 2 m before a spherical mirror; in configuration (2), an object is placed after a second off-axis paraboloid mirror. Also shown is the beam pattern for configuration (1), measured at ~23 m from the laser source and taken with a 320×240 element focal-plane array camera with 1 s integration.

The 1.97 mm long device produced a cw power of 38 mW at 9 K as measured with a thermopile detector (Scientech, model AC2500). At ~30 K, the cryocooler temperature, the device produced a peak pulsed power of ~17 mW using 13.5 ms long pulses at 27% duty cycle. This pulsed bias scheme is required for synchronization with the readout of the microbolometer camera for differential imaging in order to subtract the strong infrared background from the terahertz signal.[6] The use of a shorter device resulted in a small reduction in power from 18.5 to 17 mW, due to an increase in the threshold and a smaller device size, for the 3.05 and 1.97 mm long devices, respectively. However, this lower power is more than compensated for in increased atmospheric transmission. Using distributed-feedback grating structures to "force" the lasers to oscillate at a frequency away from the gain peak could achieve the same frequency selectivity and yield a similar reduction in output power levels.

The experimental setup for long-range imaging is shown in Fig. 2. The QCL was indium soldered to a copper carrier and mounted in the cryocooler. The emitted light was collected and collimated by an $f/1$ off-axis parabolic mirror with a 5 cm diameter. Four plane mirrors (not shown) were used to fold the optical path and to direct the beam to a 15 cm diameter spherical mirror, tilted off the optical axis to prevent subsequent optical elements from obscuring the beam. In configuration (1), an $f/3$, high-resistivity Si lens was used to focus the light transmitted through an object placed at 2 m in front of the spherical mirror onto a 320 ×240 microbolometer focal-plane array [optical noise equivalent power (NEP) ~320 pW/$\sqrt{\text{Hz}}$ at 4.3 THz].[6] Note

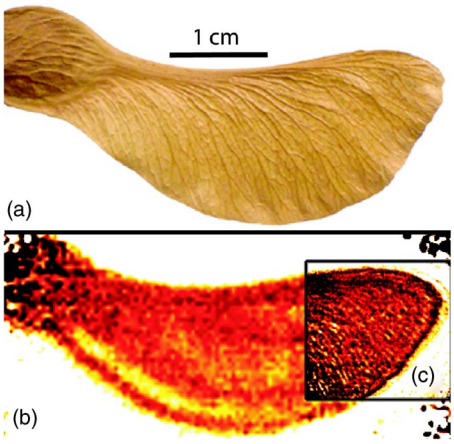

FIG. 3. (Color online) Sample images of a dried seed pod: (a) image at visible frequency, (b) terahertz image taken with configuration (1), and (c) terahertz image taken with configuration (2). Both (b) and (c) are taken with 1 s integration (average of 20 frames).

that in the object plane, which is ~23 m from the laser source, the beam pattern is highly symmetric as measured by the focal-plane array camera with 1 s integration time. In configuration (2), the reflected beam from the spherical mirror was further focused by an $f/2$ off-axis parabolic mirror and was used to back illuminate a smaller object. Transmitted light was collected and focused by an $f/1$ high-resistivity Si lens onto the focal-plane array.

The resulting images are shown in Fig. 3. A dried seed pod is used as the see-through object to simulate foliage penetration (FOPEN). In part (a) a white light image of the dried seed pod is shown, with the corresponding terahertz transmission images shown in parts (b) and (c) for configurations (1) and (2), respectively. After transmission over the 25.75 m path, the resulting focal-plane average SNRs were ~2.5 and 10 for a single-frame and a 20-frame average (0.05 and 1 s of integration, respectively) respectively. The 20-frame average images shown in (b) and (c) were normalized to the beam pattern and were spatially low-pass filtered to smooth out isolated pixels with low SNR. This postdetection signal processing is performed in real time and only adds an ~5 ms delay in displaying the images. The image in part (b) has low spatial resolution due to the 2 m distance from the spherical mirror, with a calculated resolution of ~3 mm at the object plane using ray tracing software (CODE V, Optical Research Associates). Part (c) shows a much higher spatial resolution, due to the closer positioning of the object to the camera. As a result, the fine ridges of the seed pod (approximately millimeter spacing) can be resolved, as predicted by the ray tracing resolution of ~0.75 mm.

The beam propagation losses were measured using optical configuration (1) with a shorter 10.1 m path to allow the use of the thermopile detector with a sufficient SNR. The thermopile was used at the focal point of the 15 cm mirror, without a Si lens. Power measurements were taken immediately after the off-axis paraboloid (OAP) and after the 10.1 m path. The propagation loss was determined to be $0.79 \pm .03$ dB/m, somewhat larger than the predicted loss of $0.52 \pm .05$ dB/m, which was calculated using the experimental conditions of 292 K and $(48 \pm 5)\%$ RH. Some of these losses were likely due to divergence of higher-order spatial modes, whose power was included in the measurement after the first OAP. In fact, the beam pattern measured immediately after the first OAP is far less symmetric than that shown in Fig. 2, indicating that most of the higher-order spatial modes have been "filtered out" after a long distance (>10 m). Additional losses were likely due to imperfect mirror reflectivity of the four folding mirrors and absorption by the protective coating of the 15 cm spherical mirror.

Using the calculated path loss of 0.79 dB/m, it is estimated that ~150 μW reaches the object after ~25.8 m, which is still sufficient for penetrating the dried seed pod for imaging with the microbolometer camera. Optimization of the microbolometer camera specifically for terahertz frequencies could reduce the optical NEP and thus improve SNR by two orders of magnitude, from ~320 to several pW/$\sqrt{\text{Hz}}$ that is close to its measured electrical NEP of ~1 pW/$\sqrt{\text{Hz}}$.[10] Further sensitivity improvements could be made by using cooled detectors such as the terahertz quantum well infrared photodetector[11] and the use of higher power QCLs. Both improvements will lead to a linear increase of SNR. Exponential improvements can be made by utilizing atmospheric transmission windows at lower frequencies, most notably the ~1.5 THz window (~0.23 dB/m at 296 K and 40% RH), which has the lowest absorption in the 1–5 THz range. The lower frequencies are also beneficial for better penetration of optically dense materials such as clothes and leaves. Presently, QCLs have already been developed at 1.59 THz.[5] With further improvement in frequency and power outputs and the use of higher sensitivity detectors, it is conceivable that terahertz imaging can be performed over a standoff range in reflection mode similar to Ref. 12, with real-time frame rates and no moving parts. In conclusion, our work has demonstrated that terahertz QCLs, because of their high-power levels and great frequency flexibility, are uniquely suited for real-time terahertz imaging over long distances.

This work is supported by AFOSR, NASA, and NSF. Sandia is a multiprogram laboratory operated by Sandia Corporation, a Lockheed Martin Company, for the United States Department of Energy under Contract No. DE-AC04-94AL85000.

[1] K. Kawase, Opt. Photonics News **15**, 34 (2004).
[2] B. B. Hu and M. C. Nuss, Opt. Lett. **20**, 1716 (1995).
[3] M. C. Kemp, P. F. Taday, B. E. Cole, J. A. Cluff, A. J. Fitzgerald, and W. R. Tribe, Proc. SPIE **5070**, 44 (2003).
[4] B. S. Williams, S. Kumar, Q. Hu, and J. L. Reno, Electron. Lett. **42**, 89 (2006).
[5] S. Kumar, B. S. Williams, Q. Qin, Q. Hu, Z. R. Wasilewski, and H. C. Liu (unpublished).
[6] A. W. M. Lee, B. S. Williams, S. Kumar, Q. Hu, and J. L. Reno, IEEE Photonics Technol. Lett. **18**, 1415 (2006).
[7] L. S. Rothman, D. Jacquemart, A. Barbe, D. C. Benner, M. Birk, L. R. Brown, M. R. Carleer, C. Chackerian, Jr., K. Chance, L. H. Coudert, V. Dana, V. M. Devi, J.-M. Flaud, R. R. Gamache, A. Goldman, J.-M. Hartmann, K. W. Jucks, A. G. Maki, J.-Y. Mandin, S. T. Massie, J. Orphal, A. Perrin, C. P. Rinsland, M. A. H. Smith, J. Tennyson, R. N. Tolchenov, R. A. Toth, J. Vander Auwera, P. Varanasi, and G. Wagner, J. Quant. Spectrosc. Radiat. Transf. **96**, 139 (2005).
[8] Q. Hu, B. S. Williams, S. Kumar, H. Callebaut, S. Kohen, and J. L. Reno, Semicond. Sci. Technol. **20**, S228 (2005).
[9] C. Sirtori, F. Capasso, J. Faist, A. L. Hutchinson, D. L. Sivco, and A. Y. Cho, IEEE J. Quantum Electron. **34**, 1722 (1998).
[10] N. Butler, R. Blackwell, R. Murphy, R. Silva, and C. Marshall, Proc. SPIE **2552**, 583 (1995).
[11] H. C. Liu, C. Y. Song, A. J. SpringThorpe, and J. C. Cao, Appl. Phys. Lett. **84**, 4068 (2004).
[12] J. C. Dickinson, T. M. Goyette, A. J. Gatesman, C. S. Joseph, Z. G. Root, R. H. Giles, J. Waldman, and W. E. Nixon, Proc. SPIE **6212**, 62120E (2006).